

## RESEARCH ARTICLE

# Multivariable Coordinated Nonlinear Gain Droop Control for PV-Battery Hybrid DC Microgrid Access System via a T-S Fuzzy Decision Approach

MAO JINGFENG, ZHANG XIAOTONG, YIN CHUNYUN, WU AIHUA, AND ZHANG XUDONG

School of Electrical Engineering, Nantong University, Nantong 226019, China

Corresponding author: Wu Aihua (wu.ah@ntu.edu.cn)

This work was supported in part by the Natural Science Research Program of Jiangsu Colleges and Universities under Grant 20KJA470002, in part by the Excellent Teaching Team of "Qinglan Project" of Jiangsu Colleges and Universities, and in part by the Science and Technology Research Program of Nantong under Grant JC2020094 and Grant MS22020022.


**ABSTRACT** The PV-Battery hybrid DC microgrid is an important structural form for distributed renewable energy microgrid applications. This paper focuses on improving the access utilization rate of PV-Battery energy and enhancing the access stability of the DC bus voltage. Firstly, based on the voltage droop control method for multi-source access system, the relationship between the power margin of PV-Battery energy and the regulation of DC bus voltage deviation is analyzed. Then, a multivariable T-S fuzzy decision approach is used to design a nonlinear virtual resistance-based voltage droop gain coefficient function, which achieves a highly adaptive coordinated distribution of PV-Battery power as well as supports DC bus voltage stabilization. The T-S fuzzy input variables include the DC bus voltage deviation of the access point, the state of charge of the battery, and the PV sunlight intensity. Finally, the simulation system is built employing MATLAB/Simulink, and the feasibility and effectiveness of the proposed strategy are verified through multi-scheme simulations.

**INDEX TERMS** Renewable energy, DC microgrid, T-S fuzzy control, variable gain, coordinated control.

## NOMENCLATURE

$P_{pv\_i}$	Output power of the $i$ th PV cell.
$P_{dc\_L}$	Consume power of the DC load.
$P_{batt\_j}$	Output power of the $j$ th battery.
$P_{RES}$	Output power of RES.
$P_{Load}$	Total consume power of the load side.
$P_{ESS}$	Total power of ESS.
$V_{sw}$	Switching voltage.
$SoC$	State of charge.
$SoC(0)$	Initial $SoC$ of the battery.
$\Delta SoC$	Battery $SoC$ variation.
$V_{batt}$	Battery voltage.
$V_{dc}$	DC bus access point voltage.
$V_H$	DC bus voltage upper threshold.

$V_L$	DC bus voltage lower threshold.
$V_{ref}$	DC bus voltage reference.
$R_v$	Virtual resistance of the battery droop control circuit.
$V_{dc\ ref}$	Battery converter output voltage reference.
$i_{dc}$	Battery converter output current.
$R_{CPS}$	Equivalent resistance of the PV.
$I_{CPS}$	Equivalent current of the PV.
$R_{load}$	DC load resistance.
$C_{batt}$	Battery capacity.
$i_{batt}$	Battery terminal current.
$\tilde{R}_v$	Battery virtual resistance control law.
$K_{V\_err}, K_{SOC}$	Gain coefficients of the battery virtual resistance control law.
$L_i$	Constant parameter of the battery membership function.

The associate editor coordinating the review of this manuscript and approving it for publication was Haibin Sun .

$\mu_P(x_i), \mu_N(x_i)$	Membership functions of the battery T-S fuzzy controller.
$v_1, v_2, v_3, v_4$	Outputs of the battery T-S fuzzy control rule.
$K_1, K_2, K_3, K_4$	Proportion coefficients of the battery T-S fuzzy control rule.
$a_1, a_2$	Combination coefficients of the battery T-S fuzzy control rule.
$u$	Output of the T-S fuzzy controller.
$F(\alpha, x_1, x_2)$	Battery gain coefficient function.
$\alpha$	Parameter of the battery variable gain coefficient function.
$F(x_1, x_2)$	Battery gain coefficient function with center-of-gravity defuzzify.
$K$	PV droop control gain coefficient.
$V_{dc\ ref}$	PV access converter output voltage reference.
$P_{dc}$	PV converter output power.
$S^*$	Sunlight intensity base value.
$S$	Actual sunlight intensity.
$\tilde{S}$	Standard value of sunlight intensity.
$G(x_1, x_2)$	PV gain coefficient function with center-of-gravity defuzzify.
$V_{err}$	DC bus access point voltage deviation.

## I. INTRODUCTION

With the gradual degradation of fossil fuels and the deepening environmental crisis, renewable energy sources such as photovoltaic electricity (PV) are widely used in distributed DC microgrid. In this case, energy storage units especially battery electricity are used to maintain a balance between fluctuating PV generation and load consumption. Balancing the PV and battery power output and preventing the battery from being deeply over-discharged or over-charged have become very important objectives in the operational control of PV-Battery hybrid DC microgrid [1], [2], [3]. For a PV-Battery hybrid DC microgrid operating independently, a coordinated control strategy needs to be well designed to keep the system work in different operating conditions, which is used to ensure system stably and reliably [4], [5], [6].

Reference [7], a coordinated control strategy for PV-Battery systems is proposed to maximize the utilization of the battery and keep the *SoC* within the desired range. Simulation results show that the bus voltage has higher stability, and the lifetime of the Li-ion and lead-acid battery are extended by 29.93% and 42.93% respectively. Reference [8], a power distribution strategy for hybrid energy storage systems based on virtual resistance is proposed. The system can achieve smooth switching within four operating modes according to different operating conditions. According to the test results, this strategy can effectively suppress the high-frequency fluctuations caused by the source power fluctuation, ensure the system power balance and maintain the DC bus voltage stability. However, the stability of the centrally controlled microgrid relies mainly on communication technology. If communication fails, the whole system is disabled.

Without the need of remote communication and a central controller, the voltage droop control method can connect multiple different sources in parallel to the microgrid, and achieve reasonable power distribution and voltage regulation among multiple sources. Droop control has been widely used in DC microgrid.

In the traditional droop control method, as the output current of each distributed source increases, its reference voltage decreases according to the fixed droop gain coefficient, which indirectly achieves an automatic power distribution of each distributed source. The disadvantage of this method is that the droop gain coefficient is fixed, which is not conducive to the expansion of the system or the optimal management of energy in DC microgrid [9], [10], [11]. The unavoidable line impedance will inevitably lead to the current sharing error of each distributed source, and will also cause the unbalance of energy storage between batteries. If a smaller droop gain coefficient is selected, the voltage deviation is not large, but the current sharing effect is poor under heavy load; if a larger droop gain coefficient is selected, the current sharing effect is good, but the bus voltage deviation is large under light load. Unbalanced current distribution accuracy and excessive voltage deviation will lead to some serious problems such as unstable bus voltage, local converter overload, and even power supply reliability failure. To solve the above problems, many papers have proposed improved control strategies [12], [13].

The secondary control method is used to compensate for the contradiction between voltage deviation and current distribution accuracy which are extensions of the traditional droop control method. The researches on the general compensation method by correlating voltage or current deviation are as follows. Reference [14] proposes a hierarchical control method with a dynamic droop coefficient correction control (DCCC) to achieve better power sharing in DC microgrid. In the proposed hierarchical control method, the DCCC is employed in the primary level, which corrects the droop coefficient automatically and the proportional current has been shared. This method has a clear idea but requires accurate prediction of circuit parameters. Reference [15] proposes a decentralized droop control method, which identifies the nonlinear droop curve coefficient with the desired bus voltage regulation and current sharing accuracy in a specified heavy load range, while a linear droop function with a negative droop resistance is used to tighten the bus voltage regulation in the light load range. This method can achieve a good light-load control effect by optimizing the droop gain coefficient, but the voltage deviation under heavy-load conditions needs to be further reduced. Reference [16] proposes a novel current-limiting droop controller for paralleled DC-DC Boost converters to guarantee closed-loop stability and power sharing, but this method did not completely eliminate the influence of mismatched line impedance on current distribution.

The optimization compensation method is an extension of the general compensation method, in which the droop gain coefficient is changed through various optimization

algorithms by relating the dynamic physical variables of the system [17]. For example, [18] uses particle swarm optimization to find the best droop coefficient. Reference [19] uses adaptive fuzzy reasoning to dynamically adjust the droop coefficient. By considering the worst points of stability as constraints, an elitist non-dominated sorting genetic algorithm is used to search the better turning points of the droop control curves, [20] proposes a multi-objective optimization segmented droop control for DC microgrid. Reference [21] introduces Petri probabilistic wavelet fuzzy neural network (PPWFNN) algorithm to optimize droop control. However, most of the above-mentioned optimization compensation algorithms rely on the communication network between the converters, and the computational load is large, which is difficult to implement on hardware devices, and is limited in practical applications.

In the isolated PV-Battery DC microgrid, it is necessary to not only enhance the stability of the DC bus voltage, but also ensure the power balance between the energy storage units to avoid any energy storage units over-discharge or over-charge. To solve this problem, in addition to changing the parameters of the droop control curve by considering changes of microgrid physical variables such as the related bus voltage deviation, it is also necessary to consider the state of charge (*SoC*) of the energy storage unit to improve the performance of droop control method.

Therefore, [22] proposes an improved droop control method based on *SoC*, but only discusses the *SoC* equilibrium when the energy storage units are discharging, and does not analyze the *SoC* equilibrium when they are charging. Reference [23] proposes an adaptive droop control method based on the fuzzy algorithm with the voltage deviation, voltage unbalance coefficient, and *SoC* as input variables, which are designed to obtain an optimized droop control coefficient. Nevertheless, during a long period of discharge process, the balance of the *SoC* cannot be determined accurately due to the slow response speed of the energy storage units. Reference [24] adopts an improved *SoC*-based power function droop control method. The droop coefficient is proportional to  $SoC^n$  when the battery is charging and inversely proportional to  $SoC^n$  when the battery is discharging. The larger  $n$  is, the faster the *SoC* equalizes. However, the above-mentioned methods have low averaging accuracy and large voltage deviation. Reference [25] adopts a droop control method based on *SoC* exponential function, the droop coefficient  $k_d$  is proportional to  $\exp[p(SoC - A_{SoC})]$  during charging, and inversely proportional to  $\exp[p(SoC - A_{SoC})]$  during discharging. The larger  $p$  is, the faster the *SoC* equalizes. However, this method does not consider reducing the bus voltage deviation generated by this process.

To sum up, most of the existing research methods do not have a strong ability to ensure that the isolated PV-Battery DC microgrid simultaneously satisfies high adaptability to coordinate the distribution of loads, balance the power of the energy storage units, and good coordination effect of supporting DC bus voltage regulation.

In particular, one of the main advantages of a fuzzy logic controller is that different control objectives can be managed simultaneously and harmoniously [26], [27]. Reference [28] uses a fuzzy algorithm to optimize the droop gain coefficient. In this case, the droop gain coefficient is adjusted according to the output power of each source, while the fuzzy logic output is the DC bus voltage reference value. The algorithm can achieve the goals of DC bus voltage regulation, current distribution, and power balancing in distributed energy storage systems. However, once a new source is added to the system, it is necessary to obtain the state information of each source through low-speed communication to adjust the membership function of the fuzzy control, which is relatively time-consuming. An improved fuzzy control strategy for DC microgrid droop control is proposed in [29]. It ensures stable operation of the system without the need to change the fuzzy logic system and without communication, and multiple control objectives can be achieved. The simulation results show that this strategy contributes to the power balance among sources and reduces the DC bus voltage deviation. However, the Mamdani-type fuzzy control used in this strategy has a long time-consuming in defuzzification process, which greatly reduces the efficiency of the system. In contrast, each output rule of the T-S fuzzy model has an exact quantity corresponding to input variables, which avoids the Mamdani-type fuzzy defuzzification process and has higher calculation efficiency [30], [31]. Reference [32] proposed an analytical structure of the T-S fuzzy logic approach to realize a nonlinear variable gain characteristic for traditional control method. Since the characteristics of the variable gain control are parameterized and controlled by the rules of proportionality, the efficiency and the computational accuracy of the fuzzy control are greatly improved.

In summary, the main contributions of this paper include: (1) For the distributed PV and battery multi-source access system, three different operation modes are designed according to the type of distributed source that is responsible for regulating the DC bus voltage. (2) Using the multivariable T-S fuzzy decision approach, two voltage droop variable gain coefficient functions based on nonlinear virtual resistance for PV and battery droop controllers are designed respectively, which take the bus voltage deviation of the access point, the *SoC* of the battery, and the sunlight intensity as input variables. (3) The nonlinear variable-gain cooperative control strategy based on the T-S fuzzy decision approach is conducive to the maximum utilization of PV power, and the coordinated distribution of PV and battery power with high adaptability, which further enhances the anti-disturbance of the DC microgrid bus voltage. (4) The feasibility and effectiveness of the proposed strategy are verified by multi-scheme digital simulation.

The paper is organized as follows: Section II describes the configuration and operation modes of the PV-Battery DC microgrid, as well as the switch conditions among the multi-operation state controllers. In Section III, two kinds of T-S fuzzy-based variable gain droop controllers for battery and

PV are designed respectively. In Section IV, four simulation schemes are designed, and the feasibility and effectiveness of the control approach proposed in this paper are verified by the simulation results. Finally, the conclusions of the research content of this paper and future research trends are introduced in Section V.

## II. CONFIGURATION AND OPERATION OF PV-BATTERY HYBRID DC MICROGRID

In general, a PV-Battery hybrid DC microgrid usually consists of three components, including RES (Photovoltaics), ESS (Batteries), and DC load, as shown in Figure 1.

RES units are used to supply power generation, and ESS units are used to maintain the power balance between generation and load. In grid-connected operation, the power of the DC microgrid can be balanced by the main grid. However, when the microgrid is operated in islanding mode, only the ESS can absorb the excess power or compensate for the deficit power.

In Figure 1,  $P_{PVi}$  represents the output power of the  $i$ th PV cell ( $i = 1, 2, \dots, m$ ),  $P_{dcL}$  represents the consume power of the DC load, and  $P_{battj}$  represents the output power of the  $j$ th battery ( $j = 1, 2, \dots, n$ ).  $P_{RES}$  is the output power of RES,  $P_{Load}$  is the total consume power of the DC load side, and  $P_{ESS}$  is the total power of ESS. Where  $m$  and  $n$  represent the number of PV and battery respectively,  $i \leq m, j \leq n$ .

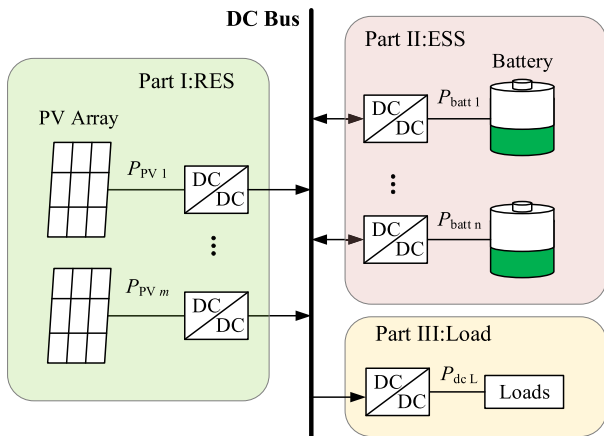


FIGURE 1. Typical configuration of PV-Battery hybrid DC microgrid.

The power equations of the DC microgrid shown in Figure 1 can be expressed as

$$\begin{aligned} P_{RES} &= \sum_{i=1}^m P_{PVi} \\ P_{Load} &= P_{dcL} \\ P_{ESS} &= \sum_{j=1}^n P_{battj} \end{aligned} \quad (1)$$

Normally, ESS can operate on charge state or discharge state, which depends on the power demand condition between the RES and the DC load. However, a prolonged power

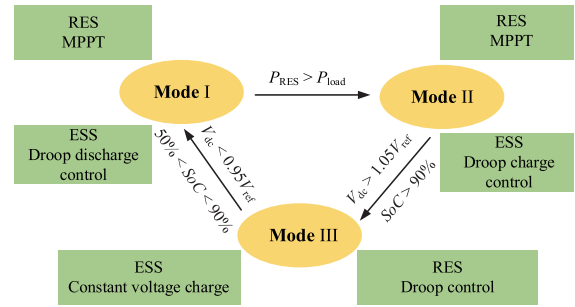


FIGURE 2. Operational model of the hybrid DC microgrid.

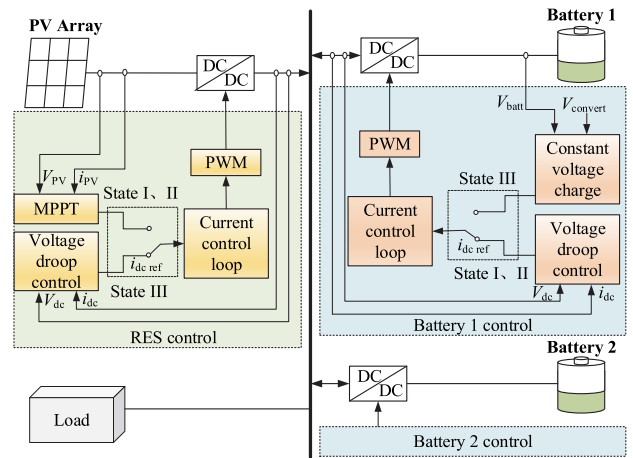


FIGURE 3. Hybrid DC microgrid control circuit under multi-operation modes switching.

unbalance between the RES and the DC load may cause the ESS to over-discharge or over-charge. To extend the lifetime of the ESS and to make full use of the RES, the paper designs three different operation modes according to the types of distributed energy sources, which are responsible for regulating the DC bus voltage, as shown in Figure 2.

The PV-Battery DC microgrid studied in the paper consists of three components, including RES (a PV access), ESS (two battery units' access), and DC load ( $R_{load}$ ). Figure 3 shows the control circuit of the DC microgrid under multi-operation modes switching. The individual operation mode and the conditions for control mode switching are illustrated in detail in this section.

### A. MODE I: PV - MPPT CONTROL AND BATTERY - DROOP DISCHARGE CONTROL

When the output power of the PV fails to supply the load, the battery can release energy to compensate for the lack of power in the DC microgrid. The power equation is expressed as

$$P_{batt} = P_{Load} P_{PV} \quad (2)$$

In Mode I, the PV operates in MPPT control state, which can be regarded as a constant power supply (CPS). At the same time, the battery operates in voltage droop control state, which is responsible for regulating the DC bus voltage.



Normally, in Mode I, the battery SoC is kept between 50% and 90%, and the battery discharges according to the power generated by the PV and the load consumption.

**B. MODE II: PV – MPPT CONTROL AND BATTERY – DROOP CHARGE CONTROL**

In Mode II, the PV operates in MPPT control state, and the PV generation is greater than the load demand, while the battery SoC is less than 50%. To make full use of renewable energy, the excess power of the PV generation is stored in the battery via droop charge control. The power equation is expressed as

$$P_{batt} = P_{PV}P_{Load} \tag{3}$$

**C. MODE III: PV – DROOP CONTROL AND BATTERY–CONSTANT VOLTAGE CHARGE CONTROL**

When the PV generates much more power than the load consumption and the battery SoC is above 90%, the battery adopts constant voltage charge control to prevent overcharge. To keep the DC bus voltage stable, the PV needs to switch from MPPT control state to voltage droop control state, while the PV is responsible for DC bus voltage regulation. The battery operates in the constant voltage charge state, so the battery can be described as a constant power load (CPL). The power equation is expressed as

$$P_{batt} \approx P_{Load} \tag{4}$$

**D. SWITCHING BETWEEN MULTI-STATE CONTROLLERS**

Since the current direction of the bi-directional DC-DC converter is reversible, the droop control circuit of the battery can realize both charge and discharge. When the battery is operating in the charge state with droop control, its terminal voltage reaches the switching voltage  $V_{sw}$  and the charger should keep the battery voltage constant to prevent it from overcharge. When the battery voltage reaches the switching voltage  $V_{sw}$ , the battery operation state switches to constant voltage charge. At this stage, the battery current gradually decreases until near zero. Once below a certain preset threshold, the battery is considered fully charged.

For the battery charge or discharge control, the switching from voltage droop discharge control (State I) to voltage droop charge control (State II) is determined by the requirement power of the microgrid system. When the output power of the PV is more than the requirement of load, the battery is switched from the discharge state to the charge state. The switching from voltage droop charge control (State II) to constant voltage charge control (State III) is determined by whether the battery voltage  $V_{batt}$  reaches the switching voltage threshold  $V_{sw}$ . The switching from constant voltage charge control (State III) to voltage droop discharge control (State I) is determined by the DC bus voltage lower-threshold  $V_L$  and the DC bus voltage reference  $V_{ref}$  ( $V_{dc} < V_L$ ,  $V_L = 0.95V_{ref}$ ). Figure 4 shows the switching conditions among the internal control states of the battery.

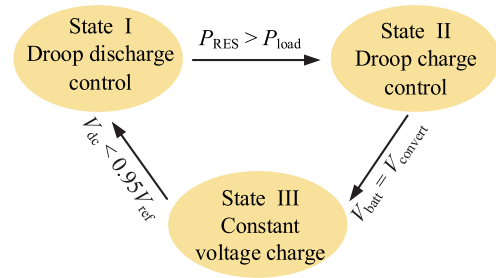


**FIGURE 4. Multi-State switching among the internal control states of the battery.**

Once any battery reaches the switching voltage threshold  $V_{sw}$ , the PV still running in MPPT control state until the DC bus voltage  $V_{dc}$  reaches the voltage upper-threshold ( $V_H = 1.05V_{ref}$ ). Then, the PV internal control switches from MPPT control to voltage droop control. At this point, the microgrid operates in Mode III.

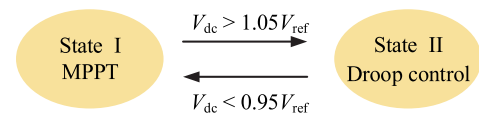


**FIGURE 5. Multi-State switching between the internal control states of the PV generation.**

For the PV generation control, the switching from MPPT control (State I) to voltage droop control (State II) and the switching from voltage droop control (State II) to MPPT (State I) are both determined by the DC bus voltage  $V_{dc}$ , which meets to the conditions of  $V_{dc} > V_H$  or  $V_{dc} < V_L$  respectively. Figure 5 shows the switching conditions for the PV controller state. The following sections focus on the design of the battery and the PV voltage droop controllers.

**III. T-S FUZZY-BASED NONLINEAR VARIABLE GAIN DROOP CONTROL**

In this section, a T-S fuzzy-based nonlinear variable gain decision approach for regulating the virtual resistance of voltage droop control is designed. The main objective is to ensure the power balance of the distributed sources, maximum utilization rate of PVs, and avoid deeply over-discharge or over-charge of battery. In addition, reducing the DC bus access point voltage deviation is another important control objective. Considering that battery and PV adopt different control states to adapt to various operation conditions of the DC microgrid, two different T-S fuzzy droop controllers are designed for battery and PV respectively.

**A. BATTERY ACCESS SYSTEM T-S FUZZY DROOP CONTROL FOR CHARGE AND DISCHARGE**

When the DC microgrid operates in Mode I and Mode II, the charge or discharge process of the battery is managed by droop control. The traditional voltage-type droop control

output expression is

$$V_{dc\ ref} = V_{ref} - i_{dc}R_v \quad (5)$$

where  $R_v$  is the virtual resistance of the battery droop control circuit, which can also be defined as a droop gain coefficient in the droop control expression;  $V_{dc\ ref}$  is the battery access converter output voltage reference value, which is generated by the battery droop control law;  $V_{ref}$  is the DC bus access point voltage reference value;  $i_{dc}$  is the battery access converter output current.

It can be seen from equation (5) that the smaller value of  $R_v$ , the more current the battery injects or absorbs, so as to maintain the DC microgrid power balance. To ensure energy balance, the battery with the lowest  $SoC$  needs to charge fastest than the other battery. In other words, the smaller the battery  $SoC$ , the smaller the  $R_v$  allocation should be. During discharge process, the battery with the highest  $SoC$  needs to discharge fastest than the other battery. Similarly, the greater the battery  $SoC$ , the greater the  $R_v$  allocation should be.

Figure 6 shows the equivalent circuit of the DC microgrid in operation Mode I and Mode II.

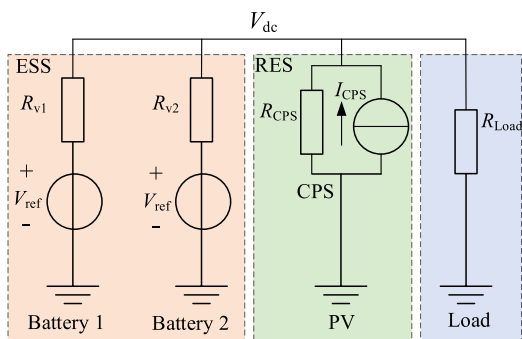


FIGURE 6. DC microgrid equivalent circuit in operation Mode I and Mode II.

In Figure 6, the CPS is represented by a constant current source and a resistance connected in parallel, and the battery droop circuit is represented by a resistance  $R_v$  and a voltage source connected in series. Where  $R_{CPS}$  is the equivalent resistance of the PV,  $I_{CPS}$  is the equivalent current of the PV, and  $R_{load}$  is the DC load resistance. By setting the DC bus access point as the node, the DC bus access point voltage  $V_{dc}$  is expressed as

$$V_{dc} = \frac{\frac{V_{ref}}{R_v} + I_{CPS}}{\frac{1}{R_v} + \frac{1}{R_{CPS}} + \frac{1}{R_{load}}} \quad (6)$$

$R_{CPS}$  and  $I_{CPS}$  can be expressed respectively as

$$R_{CPS} \approx \frac{V_{dc}^2}{P_{CPS}} \quad (7)$$

$$I_{CPS} \approx 2 \frac{P_{CPS}}{V_{dc}} \quad (8)$$

Substituting Equation (5), Equation (7), and Equation (8) into Equation (6), it has

$$V_{dc} = \frac{\frac{V_{ref}}{R_v} + \sqrt{\left(\frac{V_{ref}}{R_v}\right)^2 + 4P_{CPS}\left(\frac{1}{R_v} + \frac{1}{R_{load}}\right)}}{2\left(\frac{1}{R_v} + \frac{1}{R_{load}}\right)} \quad (9)$$

Once the range of  $V_{dc}$  has been determined, the range of the virtual resistance  $R_v$  can be obtained from Equation (9).

Assuming that the DC bus access point voltage deviation  $V_{err}$  is

$$V_{err} = V_{ref} - V_{dc} \quad (10)$$

According to Equation (5) and (10), in order to prevent the DC bus access point voltage deviation from being too large, when the absolute value of the deviation  $V_{err}$  is large, it is necessary to assign a small  $R_v$  value to the droop gain. Conversely, when the absolute value of the deviation  $V_{err}$  is small, a larger  $R_v$  value is provided to the droop gain.

The battery  $SoC$  can be estimated by the current integration approach, and its expression is

$$SoC = SoC(0) - \int_0^t \frac{i_{batt}(\tau)}{C_{batt}} d\tau \quad (11)$$

where  $SoC(0)$  represents the initial  $SoC$  of the battery;  $C_{batt}$  is the battery capacity;  $i_{batt}$  is the battery terminal current.

The battery  $SoC$  variation  $\Delta SoC$  can be expressed as

$$\Delta SoC = SoC - SoC(0) = - \int_0^t \frac{i_{batt}(\tau)}{C_{batt}} d\tau \quad (12)$$

From the balance relationship between the input and output power of the battery access converter, it has

$$i_{batt}V_{batt} = i_{dc}V_{dc} \quad (13)$$

Combining Equation (10), Equation (12), and Equation (13), it has

$$\Delta SoC = \zeta \int_0^t V_{err}(\tau) d\tau \quad (14)$$

where  $\zeta = \frac{V_{dc}}{R_v V_{batt} C_{batt}}$ .

From Equation (14), it can be seen that the battery  $SoC$  is affected by variations of the virtual resistance  $R_v$  and the DC bus access point voltage deviation  $V_{err}$ . Conversely,  $R_v$  is also affected by variations of  $SoC$  and  $V_{err}$ .

Figure 7 shows the battery access system control structure in Mode I and Mode II, which the battery operates in droop control state and the T-S fuzzy controller is used to adjust the virtual resistance  $R_v$ .

The T-S fuzzy controller can deal with different control objectives simultaneously and harmoniously. The control objectives of the battery access converter are to coordinate the power distribution of the microgrid, reduce the voltage deviation of the DC bus access point, and prevent battery from over-charge and over-discharge. According to these objectives, the T-S fuzzy controller takes the battery  $SoC$  and the DC bus access point voltage deviation  $V_{err}$  as inputs and

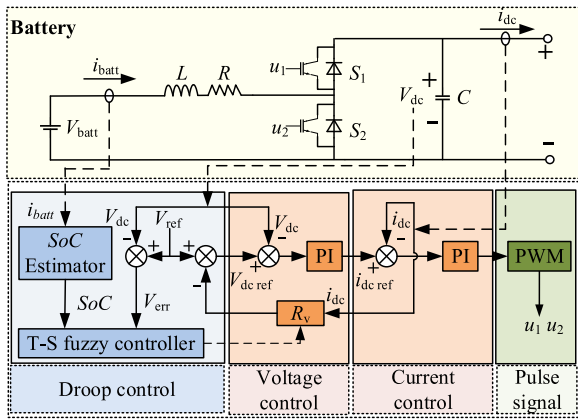


FIGURE 7. Battery access system fuzzy droop control for Mode I and Mode II.

the virtual resistance  $R_v$  of the battery droop control circuit as output.

The virtual resistance control law  $\tilde{R}_v$  is designed as

$$\tilde{R}_v = K_{V_{err}} V_{err} + K_{SoC} SoC \quad (15)$$

where  $K_{V_{err}}$  and  $K_{SoC}$  are the gain coefficients of the battery virtual resistance control law  $\tilde{R}_v$ .

As shown in Figure 8, the DC bus access point voltage deviation  $V_{err}$  and the battery  $SoC$  are both used as T-S fuzzy input variables. The input variables are fuzzified by two fuzzy sets Pos and Neg with the semi-trapezoidal distribution membership function.

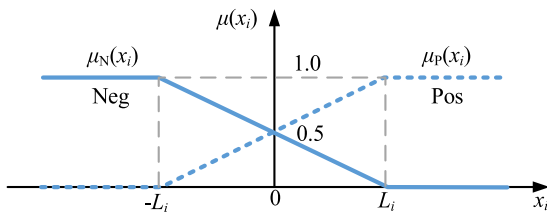


FIGURE 8. Membership function.

where,  $i = 1, 2$ , define  $x_1 = V_{err}$ ,  $x_2 = SoC$ .  $L_i$  are the constant parameters of the membership functions. The corresponding expressions for the membership functions are

$$\mu_P(x_i) = \begin{cases} 0, & x_i < -L_i \\ \frac{x_i + L_i}{2L_i}, & -L_i < x_i < L_i \\ 1, & x_i > L_i \end{cases} \quad (16)$$

$$\mu_N(x_i) = \begin{cases} 1, & x_i < -L_i \\ \frac{-x_i + L_i}{2L_i}, & -L_i < x_i < L_i \\ 0, & x_i > L_i \end{cases} \quad (17)$$

The fuzzy controller uses the following four simplified linear T-S fuzzy control rules:

Rule 1 : If  $V_{err}$  is Pos and  $SoC$  is Pos, then

$$v_1 = K_1(a_1 V_{err} + a_2 SoC)$$

Rule 2 : If  $V_{err}$  is Pos and  $SoC$  is Neg, then  $v_2 = K_2 v_1$

Rule 3 : If  $V_{err}$  is Neg and  $SoC$  is Pos, then  $v_3 = K_3 v_1$

Rule 4 : If  $V_{err}$  is Neg and  $SoC$  is Neg, then  $v_4 = K_4 v_1$

$$(18)$$

In the T-S fuzzy control rules,  $v_j$  represent the outputs of the controller,  $j = 1, 2, 3, 4$ . Using the generalized defuzzification approach, the final output  $u$  of the T-S fuzzy controller can be expressed as

$$u = \frac{\sum_{j=1}^4 (\mu_j)^\alpha v_j}{\sum_{j=1}^4 (\mu_j)^\alpha} = F(\alpha, x_1, x_2) (a_1 V_{err} + a_2 SoC) \quad (19)$$

$$\text{where } F(\alpha, x_1, x_2) = \frac{K_1(\mu_1^\alpha + \mu_2^\alpha K_2 + \mu_3^\alpha K_3 + \mu_4^\alpha K_4)}{\mu_1^\alpha + \mu_2^\alpha + \mu_3^\alpha + \mu_4^\alpha}.$$

Different defuzzification results can be obtained by using different values of  $\alpha$  ( $0 \leq \alpha \leq \infty$ ). The center-of-gravity approach and the maximum mean approach are two special defuzzification cases of  $\alpha = 1$  and  $\alpha = \infty$ , respectively.

It is obvious from Equation (19) that the T-S fuzzy controller implements a highly nonlinear variable gain coefficient control approach. The characteristics of its variable gain is determined by the nonlinear function  $F(\alpha, x_1, x_2)$ , which is determined by  $\alpha$ ,  $K_j$ ,  $L_i$ , and the dynamic real-time input  $x_i$ .

The paper uses the center-of-gravity approach to defuzzify with the selection of  $\alpha = 1$ . The output of the T-S fuzzy controller is expressed as

$$u = \frac{\sum_{j=1}^4 \mu_j \cdot v_j}{\sum_{j=1}^4 \mu_j} = F(x_1, x_2) (a_1 V_{err} + a_2 SoC) \quad (20)$$

$$\text{where } F(x_1, x_2) = \frac{K_1(\mu_1 + \mu_2 K_2 + \mu_3 K_3 + \mu_4 K_4)}{\mu_1 + \mu_2 + \mu_3 + \mu_4}.$$

By comparing Equation (15) and Equation (20), the coefficients of the virtual resistance control law  $\tilde{R}_v$  can be expressed as

$$\tilde{K}_{V_{err}}(x_1, x_2) = a_1 F(x_1, x_2) \quad (21)$$

$$\tilde{K}_{SoC}(x_1, x_2) = a_2 F(x_1, x_2) \quad (22)$$

A stable fuzzy control system operates mostly in the region around the balance point of the system  $(x_1, x_2) = (0, 0)$ . The T-S fuzzy-based variable gain droop controller is also designed by optimizing the conventional droop controller at the balance point  $(0, 0)$  of the system.

When  $x_1 = x_2 = 0$ ,

$$F(0, 0) = \frac{K_1(0.5 + 0.5K_2 + 0.5K_3 + 0.5K_4)}{0.5 + 0.5 + 0.5 + 0.5} = \frac{K_1(1 + K_2 + K_3 + K_4)}{4}.$$

To make the variable gain  $\tilde{K}_{V_{err}}(0, 0)$  and  $\tilde{K}_{SoC}(0, 0)$  of the droop control law at the balance point coincide with the

conventional gain coefficient of the virtual resistance control law  $K_{V_{err}}$  and  $K_{SoC}$ , it has

$$\tilde{K}_{V_{err}}(0, 0) = K_{V_{err}} = a_1 F(0, 0) \quad (23)$$

$$\tilde{K}_{SoC}(0, 0) = K_{SoC} = a_2 F(0, 0) \quad (24)$$

The weighting coefficients  $K_j$  shown in Equation (18) for the fuzzy rules are selected according to the requirements of the control objectives so that the coefficients  $a_1$  and  $a_2$  can be uniquely determined. The desired battery nonlinear variable gain droop control function  $F(x_1, x_2)$  can be well constructed by adjusting the parameters of membership functions  $L_i$  appropriately according to the actual physical meaning and characteristics of the control system input variables.

Taking the Rule 1 and Rule 4 in Equation (18) as the leading factors, the weighting coefficients are taken as  $K_1 = 1$ ,  $K_2 = K_3 = 0$  and  $K_4 = 1/3$  respectively. Then,  $a_1 = 3K_{V_{err}}$  and  $a_2 = 3K_{SoC}$  can be obtained, and the surfaces of function  $F(x_1, x_2)$  can be shown in Figure 9.

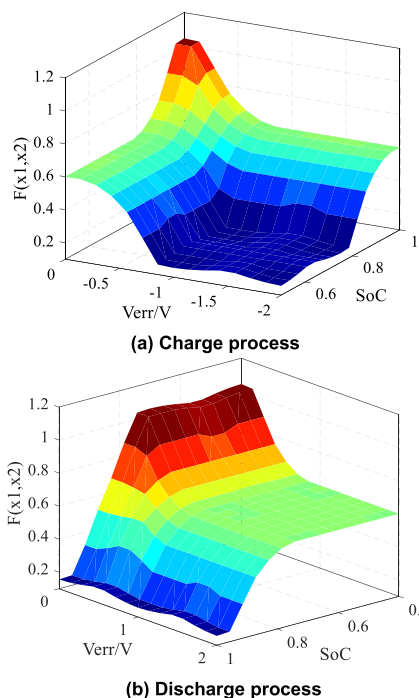


FIGURE 9. Battery fuzzy droop variable gain coefficient function  $F(x_1, x_2)$  surface.

Figure 9 (a) and (b) show the processes of charge and discharge of the battery respectively. In Figure 9 (a), the battery operates in droop charge state, which shows that the variable gain coefficient function  $F(x_1, x_2)$  has a small gain when the absolute value of  $V_{err}$  is large or the  $SoC$  is small. Correspondingly, the variable gain coefficient function  $F(x_1, x_2)$  has a large gain and is limited but not bounded, when the absolute value of  $V_{err}$  is small or the  $SoC$  is large. In Figure 9 (b), the battery operates in discharge state, which shows that the coefficient function  $F(x_1, x_2)$  has a small gain when the  $SoC$  is large. When the battery starts to discharge and the  $SoC$  gradually decreases, the variable gain coefficient

function  $F(x_1, x_2)$  gradually increases and becomes stable. When the membership function variable value of the voltage deviation  $V_{err}$  is between 0 and 1, with the decrease of  $V_{err}$ ,  $F(x_1, x_2)$  gradually increases to 1 and does not cross the boundary.

It can be seen that the adjustment rule of the  $F(x_1, x_2)$  function conforms to the principle of assigning the virtual resistance  $R_v$  of the droop control loop according to the battery  $SoC$  and the DC bus access point voltage deviation  $V_{err}$  in the process of battery charge and discharge droop control, and effectively utilizes the DC bus access point voltage deviation and prevents its value from being too large.

Figure 9 summarizes the inference rules based on the T-S fuzzy system proposed in this section, and the variable gain coefficient function  $F(x_1, x_2)$  is adjusted according to the inference rules. From Equation (14) and Equation (15), it can be seen that the virtual resistance  $R_v$  of the droop control circuit is decided according to the coefficient function  $F(x_1, x_2)$ , which are influenced by the battery  $SoC$  and the DC bus access point voltage deviation  $V_{err}$ . It is clear that the DC bus access point voltage deviation  $V_{err}$  plays an important role in the dynamic adjustment process performance. That is why the fuzzy control system tries to reduce the DC bus access point voltage deviation but not to eliminate it.

The T-S fuzzy-based non-linear variable gain droop control block diagram for battery access system is shown in Figure 10.

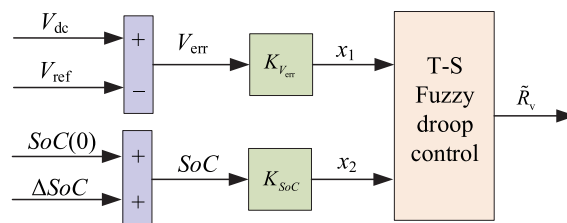


FIGURE 10. Non-linear variable gain fuzzy droop control block diagram for battery access system.

### B. PV ACCESS SYSTEM T-S FUZZY DROOP CONTROL FOR REGULATING VOLTAGE

When the microgrid system is operating in Mode III, PV is responsible for regulating the DC bus voltage. In Mode III, PV operates in droop control state. The battery operates in constant voltage charge control state, which can be represented as a constant power load (CPL). Figure 11 shows the equivalent circuit for the DC microgrid system operating in Mode III.

The PV droop control aims to adjust the generated power according to the load power demand to keep the DC bus access point voltage stable. The traditional power-type droop control output expression is

$$V_{dc\ ref'} = V_{ref} - KP_{dc} \quad (25)$$

where  $K$  is the PV droop control gain coefficient;  $V_{dc\ ref'}$  is the PV access converter output voltage reference value, which



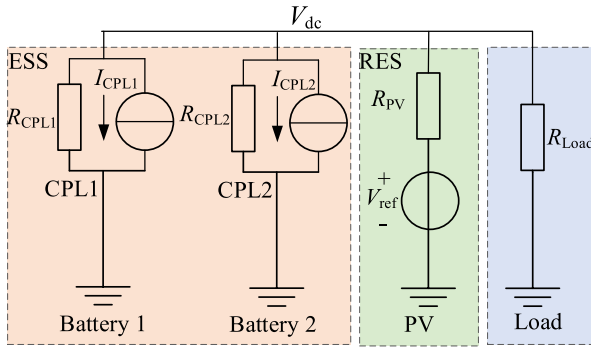


FIGURE 11. DC microgrid system equivalent circuit in operation Mode III.

is generated by the PV droop control law;  $P_{dc}$  is the output power of the PV access converter. Figure 12 shows the PV access system fuzzy droop control structure.

Assuming the sunlight intensity base value  $S^*$  is 1000 Lux, the standard value of sunlight intensity can be expressed as

$$\tilde{S} = \frac{S}{S^*} \quad (26)$$

where  $S$  is the actual sunlight intensity,  $\tilde{S} \in (0, 1)$ .

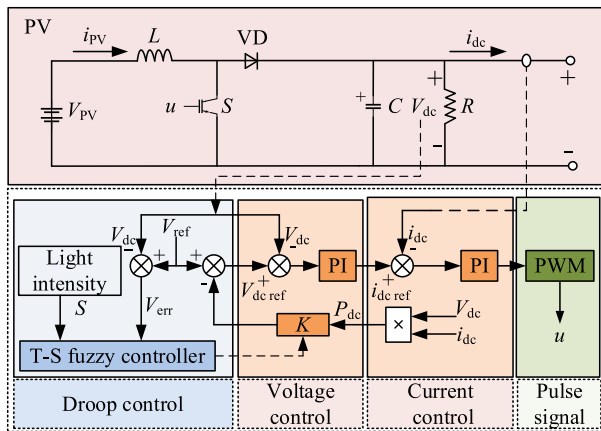


FIGURE 12. PV access system fuzzy droop control for Mode III.

Similar to the design of the battery droop control method in Section III.A, better voltage regulation and power distribution can be obtained by adjusting the droop gain coefficient  $K$  of the PV access system, which is not presented in detail here redundantly. The PV fuzzy droop variable gain coefficient function  $G(x_1, x_2)$  surface is shown in Figure 13.

As shown in Figure 13, when the absolute value of  $V_{err}$  is large, the variable gain coefficient function  $G(x_1, x_2)$  has relatively small gain. Conversely, when the absolute value of  $V_{err}$  is small, the variable gain coefficient function  $G(x_1, x_2)$  has relatively large gain. As the sunlight intensity gradually increases and the output power of the PV increases accordingly, the variable gain coefficient function  $G(x_1, x_2)$  needs to have a smaller gain to maintain the DC bus access point voltage stability. The PV droop gain coefficient  $K$  has been

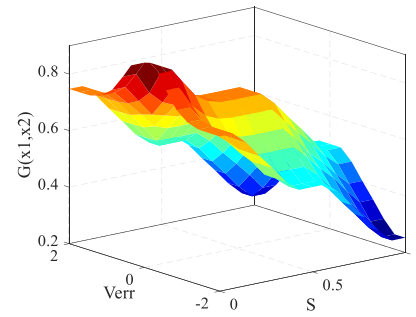


FIGURE 13. PV fuzzy droop variable gain coefficient function  $G(x_1, x_2)$  surface.

adjusted accordingly to the variation of the variable gain coefficient function  $G(x_1, x_2)$ , the sunlight intensity  $S$ , and the DC bus access point voltage deviation  $V_{err}$  to suppress external disturbances and maintain the DC bus access point voltage stability.

#### IV. SYSTEM SIMULATION AND ANALYSIS

The MATLAB/Simulink simulation platform is used to verify the feasibility and effectiveness of the proposed control strategy. The PV-Battery hybrid DC microgrid system includes a PV, two battery units, and a DC load, whose parameters are shown in Table 1. The rated voltage of the DC bus is 380V.

Four simulation schemes are designed in this section, containing three operation modes of the hybrid DC microgrid system. By changing variables such as sunlight intensity and DC load, the anti-disturbance performance of the system in Mode I, Mode II and Mode III are verified respectively. In Modes I and II, the PV setting to suddenly break down and disconnect from the microgrid access point in case of operation failure, while the battery independent power supply simulation schemes are performed to verify the complementarity and stability of the PV-Battery hybrid DC microgrid. In order to verify that the proposed strategy has over-charge protection for the battery during the charging process, the battery output power dynamic performance is simulated during the modes switching process between Mode II and Mode III.

TABLE 1. DC microgrid model parameters.

Parameter name	Numerical values	Parameter name	Numerical values
Battery rated voltage	200V	PV short-circuit current	18.68A
Battery rated capacity	6.5Ah	PV maximum power voltage	200.18V
Battery initial SoC(0)	80%	PV maximum power current	15.43A
PV open-circuit voltage	250.43V	PV maximum power	3kW

#### A. SCHEME 1: SIMULATION OF ANTI-DISTURBANCE PERFORMANCE IN MODE I AND MODE II

In this scheme, the PV operates in MPPT control state, while the battery operates in droop control state and is responsible

for regulating the DC bus voltage. This simulation scheme analyzes the dynamic process of DC bus access point voltage and PV-Battery power output, in the case of sunlight intensity changes suddenly and DC load consume power fluctuates greatly. The simulation results are shown in Figure 14.

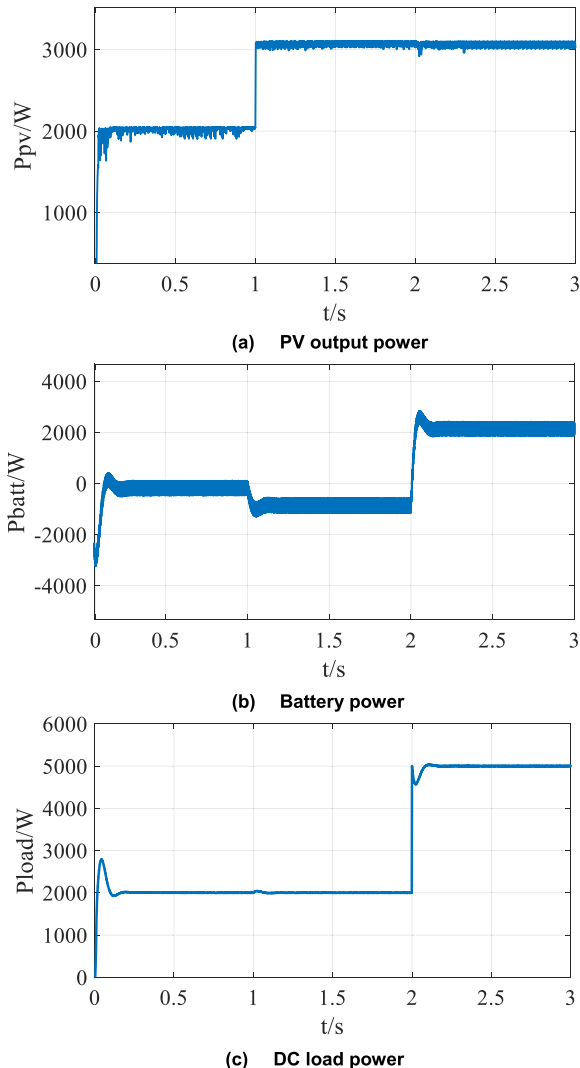


**FIGURE 14.** Operating characteristics of the hybrid DC microgrid in Scheme 1.

As shown in Figure 14, from time 0s to 1s, with a sunlight intensity of 700 Lux, the PV output power is approximately 2kW, which is close to the DC load consume power. And the battery operation state is neither charge nor discharge. At time 1s, the sunlight intensity changes from 700 Lux to 1000 Lux suddenly, and the PV output power jumps to 3kW, which is greater than the DC load consume power, and the battery operates in droop charge control state (Mode II). At time 2s, the load power changes suddenly from 2kW to 5kW and the PV output power is insufficient to meet the DC load consume power requirement. At this time, the battery switches to droop discharge control state (Mode I)

immediately, providing approximately 2kW of power to the DC load to balance the system power and maintain the DC bus access point voltage stability.

Figure 15 shows the dynamic adjustment process of the DC bus access point voltage when the system is subjected to external disturbances such as the suddenly change of PV output power and the fluctuation of DC load consume power at 1s and 2s, respectively. The simulation results show that when the battery uses the proposed T-S fuzzy variable gain droop control strategy, the DC bus access point voltage fluctuation is small and the adjustment response speed is fast.

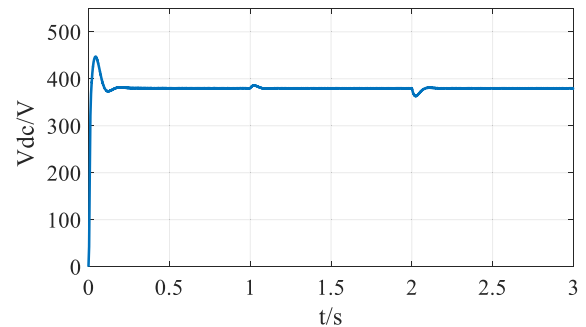


**FIGURE 15.** DC Bus Voltage for Scheme 1.

## B. SCHEME 2: SIMULATION OF BATTERY INDEPENDENT OPERATION IN MODE I AND MODE II

In this scheme, the PV operates in MPPT control state, while the battery operates in droop control state and is responsible for regulating the DC bus voltage. This simulation scheme analyzes the dynamic adjustment process and its stability capability of the system when the PV breaks down and disconnects from the microgrid access point suddenly. The simulation results are shown in Figure 16.

As shown in Figure 16, the PV operates in MPPT control state from time 0s to 1s with an output power approximately 2.4 kW. As the DC load consume power is approximately 1kW, the battery operates in droop charge control state (Mode II) to absorb excess power. At time 1s, the PV breaks down and disconnect from the microgrid access point suddenly, which its output power drops to zero. The battery changes from droop charge control state to droop discharge control state (Mode I) swiftly to adjust the output power to meet the demand of the DC load. To ensure the hybrid DC microgrid operates normally and to maintain the DC bus voltage stability, the battery output power at this point is approximately 1kW.

In Figure 17, when the PV breaks down and disconnects from the microgrid access point suddenly, the battery adjusts the power quickly via T-S fuzzy-based nonlinear variable gain droop control. The simulation results show that the DC bus access point voltage fluctuation is small, the adjustment response speed is fast, and the stability of the DC microgrid is strong.

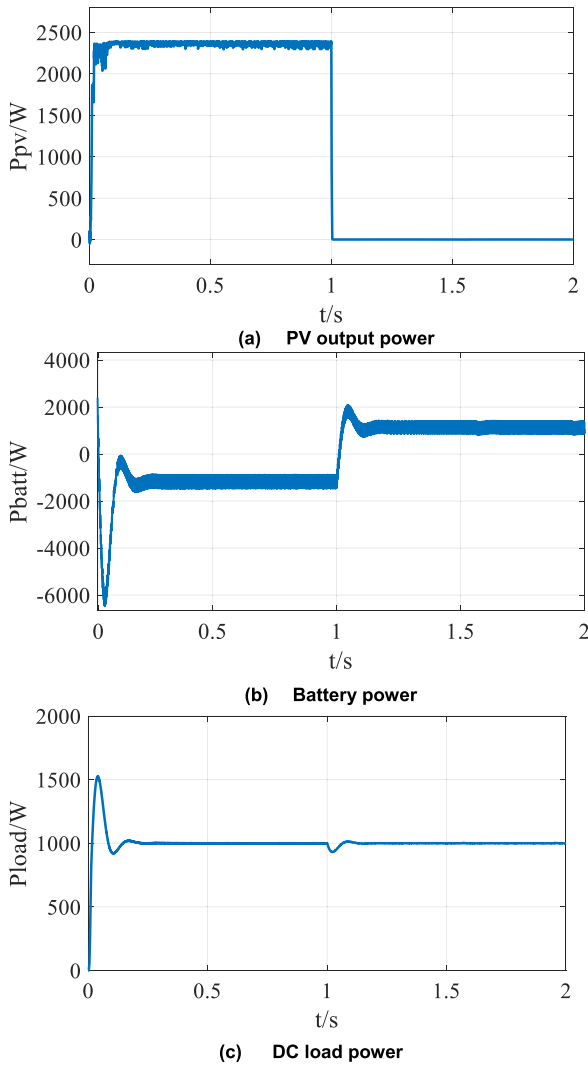


FIGURE 16. Operating characteristics of the hybrid DC microgrid in Scheme 2.

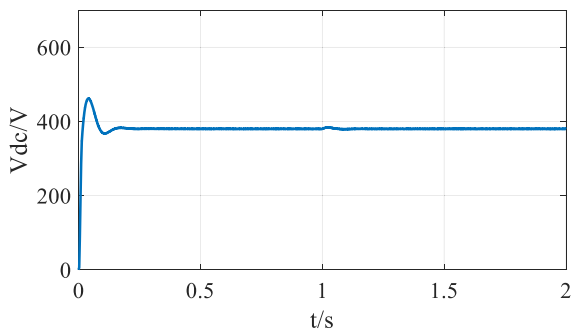


FIGURE 17. DC Bus Voltage for Scheme 2.

C. SCHEME 3: SIMULATION OF ANTI-DISTURBANCE PERFORMANCE IN MODE III

When the PV power generation is much greater than the DC load power consume, and the battery SoC is above 90%, the battery is operating in constant voltage charge control

state to prevent overcharge. To maintain the DC bus access point voltage stability, the PV operates in T-S fuzzy-based nonlinear variable gain droop control state (Mode III) which is responsible for regulating the DC bus voltage. The purpose of this simulation scheme is to analyze the influence of DC load power fluctuation for the system stability under this condition. The simulation results are shown in Figure 18.

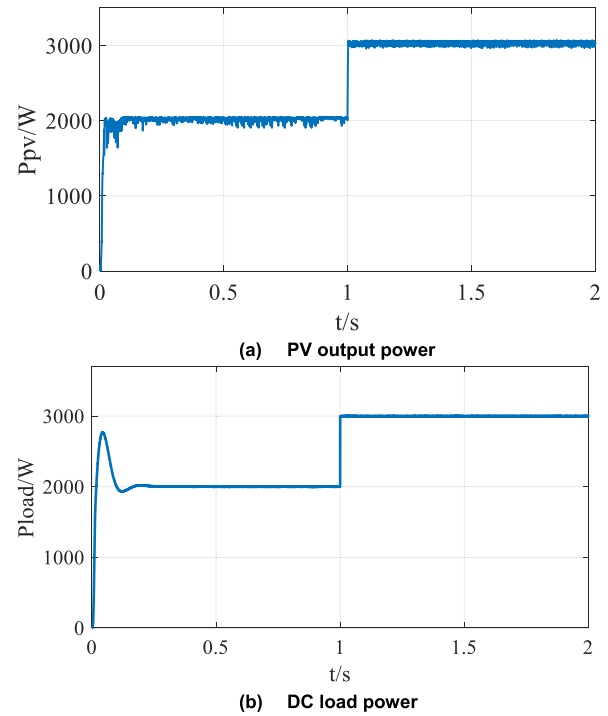


FIGURE 18. Operating characteristics of the hybrid DC microgrid in Scheme 3.

As shown in Figure 18, when the battery SoC reaches its capacity limit at time 0s to 1s, the battery is disconnected from the microgrid access point, and the PV operates in T-S fuzzy-based nonlinear variable gain droop control state (Mode III) to regulate the DC bus voltage. At time 1s, the DC load consume power changes suddenly and the PV adjusts the generation power quickly to meet the demand of the microgrid power balance.

It can be seen from Figure 19 that the switching between the MPPT control state and the T-S fuzzy-based nonlinear variable gain droop control state of the PV generation is beneficial to the reliable operation of the hybrid DC microgrid and the maintenance of DC bus access point voltage stability.

D. SCHEME 4: SIMULATION OF BATTERY PERFORMANCE UNDER MODE II AND MODE III CONVERSION CONDITIONS

At the initial moment, the PV operates in the MPPT control state, and the battery operates in the T-S fuzzy nonlinear variable gain droop charge control state. At a certain moment, when the battery SoC reaches 90% and the battery terminal voltage  $V_{batt}$  reaches the switching voltage threshold  $V_{sw}$ , the

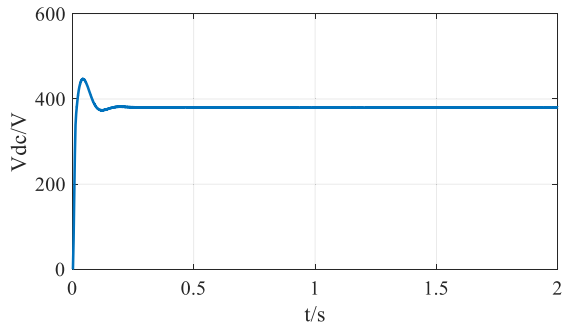


FIGURE 19. DC bus voltage of scheme 3.

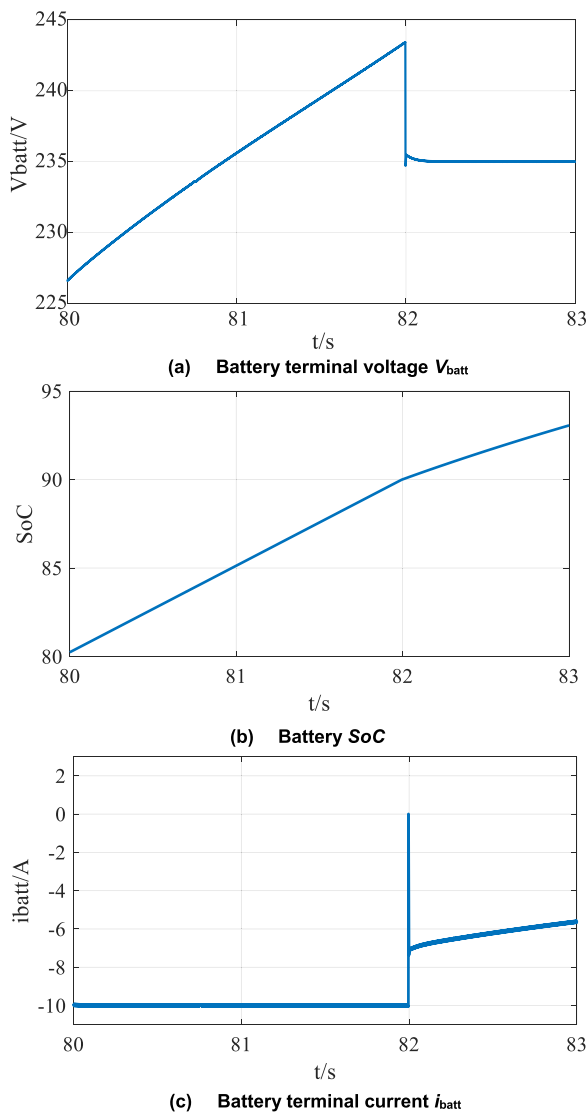


FIGURE 20. Battery characteristic curves on the switching from Mode II to Mode III.

battery switches from the variable gain droop charge control state (Mode II) to the constant voltage charge control state (Mode III). This simulation scheme demonstrates the good battery charge characteristics for this process.

As shown in Figure 20 (a) and (b), at time 82s, the battery *SoC* reaches 90% and the battery terminal voltage  $V_{batt}$  reaches the switching voltage threshold  $V_{sw}$ . At this point, the battery operating state switches from T-S fuzzy-based nonlinear variable gain droop charge control state (Mode II) to constant voltage charge control state (Mode III). In Figure 20(c), it can be seen that, at time 82s, the battery operates in the constant voltage charge state when the battery charge current decreases slowly and approaches the full state eventually. The switching of the battery control state is beneficial to balance the energy storage and prolong the life of the battery, thereby improving the reliability of the hybrid DC microgrid system.

## V. CONCLUSION

This paper proposes a multivariable coordinated nonlinear gain droop control for PV-Battery hybrid DC microgrid access system via a T-S fuzzy decision approach. According to the types of distributed energy sources and the function of regulating the DC bus voltage, three kinds of operation modes are designed. Then, a multivariable T-S fuzzy decision approach is used to construct a nonlinear virtual resistance-based voltage droop gain coefficient function, which achieves a highly adaptive coordinated distribution of PV-Battery power. When the hybrid DC microgrid is subjected to external disturbances, such as the rapidly power change of PV generation, the suddenly breakdown of PV system from operation due to faults, and the greatly fluctuation of DC load power, the distributed energy sources responsible for support the DC bus access point voltage can adjust the output power quickly to ensure the normal operation of the system and maintain the access point DC bus voltage stability. The multi-scheme simulation results show that the proposed control strategy is beneficial to the efficient access utilization rate of PV energy, effectively prevents the over-charge and over-discharge of the battery, enhances the anti-disturbance dynamic regulation characteristics of the DC bus access point voltage, and greatly improves the access stability of the hybrid DC microgrid. For future research, more robust controllers should be applied, so that the voltage and current controllers have stronger anti-interference ability and higher control accuracy.

## REFERENCES

- [1] S. Angadi, U. R. Yaragatti, Y. Suresh, and A. B. Raju, "Comprehensive review on solar, wind and hybrid wind-PV water pumping systems—An electrical engineering perspective," *CPSS Trans. Power Electron. Appl.*, vol. 6, no. 1, pp. 1–19, Mar. 2021, doi: [10.24295/CPSSSTPEA.2021.00001](https://doi.org/10.24295/CPSSSTPEA.2021.00001).
- [2] Y. S. Perdana, S. M. Muyeen, A. Al-Durra, H. K. Morales-Paredes, and M. G. Simões, "Direct connection of supercapacitor–battery hybrid storage system to the grid-tied photovoltaic system," *IEEE Trans. Sustain. Energy*, vol. 10, no. 3, pp. 1370–1379, Jul. 2019, doi: [10.1109/TSTE.2018.2868073](https://doi.org/10.1109/TSTE.2018.2868073).
- [3] X. Li, L. Wang, N. Yan, and R. Ma, "Cooperative dispatch of distributed energy storage in distribution network with PV generation systems," *IEEE Trans. Appl. Supercond.*, vol. 31, no. 8, Nov. 2021, Art. no. 0604304, doi: [10.1109/TASC.2021.3117750](https://doi.org/10.1109/TASC.2021.3117750).
- [4] D.-H. Dam and H.-H. Lee, "A power distributed control method for proportional load power sharing and bus voltage restoration in a DC microgrid," *IEEE Trans. Ind. Appl.*, vol. 54, no. 4, pp. 3616–3625, Jul./Aug. 2018, doi: [10.1109/TIA.2018.2815661](https://doi.org/10.1109/TIA.2018.2815661).



- [5] F. Li, Z. Lin, Z. Qian, J. Wu, and W. Jiang, "A dual-window DC bus interacting method for DC microgrids hierarchical control scheme," *IEEE Trans. Sustain. Energy*, vol. 11, no. 2, pp. 652–661, Apr. 2020, doi: [10.1109/TSST.2019.2900617](https://doi.org/10.1109/TSST.2019.2900617).
- [6] Y. Han, X. Ning, P. Yang, and L. Xu, "Review of power sharing, voltage restoration and stabilization techniques in hierarchical controlled DC microgrids," *IEEE Access*, vol. 7, pp. 149202–149223, 2019, doi: [10.1109/ACCESS.2019.2946706](https://doi.org/10.1109/ACCESS.2019.2946706).
- [7] H. W. Yan, A. Narang, H. D. Tafti, G. G. Farivar, S. Ceballos, and J. Pou, "Minimizing energy storage utilization in a stand-alone DC microgrid using photovoltaic flexible power control," *IEEE Trans. Smart Grid*, vol. 12, no. 5, pp. 3755–3764, Sep. 2021, doi: [10.1109/TSG.2021.3073370](https://doi.org/10.1109/TSG.2021.3073370).
- [8] H. Jidong, W. Haitao, and J. Boyuan, "Coordination control strategy for multi-mode photovoltaic and energy storage DC micro-grid," in *Proc. 6th Asia Conf. Power Electr. Eng. (ACPEE)*, Chongqing, China, Apr. 2021, pp. 688–692, doi: [10.1109/ACPEE51499.2021.9436833](https://doi.org/10.1109/ACPEE51499.2021.9436833).
- [9] V. Nasirian, A. Davoudi, F. L. Lewis, and J. M. Guerrero, "Distributed adaptive droop control for DC distribution systems," *IEEE Trans. Energy Convers.*, vol. 29, no. 4, pp. 944–956, Dec. 2014, doi: [10.1109/TEC.2014.2350458](https://doi.org/10.1109/TEC.2014.2350458).
- [10] J. Kumar, A. Agarwal, and V. Agarwal, "A review on overall control of DC microgrids," *J. Energy Storage*, vol. 21, pp. 113–138, Feb. 2019, doi: [10.1016/j.est.2018.11.013](https://doi.org/10.1016/j.est.2018.11.013).
- [11] A. Khorsandi, M. Ashourloo, and H. Mokhtari, "A decentralized control method for a low-voltage DC microgrid," *IEEE Trans. Energy Convers.*, vol. 29, no. 4, pp. 793–801, Dec. 2014, doi: [10.1109/TEC.2014.2329236](https://doi.org/10.1109/TEC.2014.2329236).
- [12] S. Golshannavaz and V. Morteznpour, "A generalized droop control approach for islanded DC microgrids hosting parallel-connected DERs," *Sustain. Cities Soc.*, vol. 36, pp. 237–245, Jan. 2018, doi: [10.1016/j.scs.2017.09.038](https://doi.org/10.1016/j.scs.2017.09.038).
- [13] P. Prabhakaran, Y. Goyal, and V. Agarwal, "Novel nonlinear droop control techniques to overcome the load sharing and voltage regulation issues in DC microgrid," *IEEE Trans. Power Electron.*, vol. 33, no. 5, pp. 4477–4487, May 2018, doi: [10.1109/TPEL.2017.2723045](https://doi.org/10.1109/TPEL.2017.2723045).
- [14] Y. Han, X. Ning, L. Li, P. Yang, and F. Blaabjerg, "Droop coefficient correction control for power sharing and voltage restoration in hierarchical controlled DC microgrids," *Int. J. Electr. Power Energy Syst.*, vol. 133, Dec. 2021, Art. no. 107277, doi: [10.1016/j.ijepes.2021.107277](https://doi.org/10.1016/j.ijepes.2021.107277).
- [15] Y. Zhang, X. Qu, M. Tang, R. Yao, and W. Chen, "Design of nonlinear droop control in DC microgrid for desired voltage regulation and current sharing accuracy," *IEEE J. Emerg. Sel. Topics Circuits Syst.*, vol. 11, no. 1, pp. 168–175, Mar. 2021, doi: [10.1109/JETCAS.2021.3049810](https://doi.org/10.1109/JETCAS.2021.3049810).
- [16] A.-C. Braiton, G. C. Konstantopoulos, and V. Kadiramanathan, "Current-limiting droop control design and stability analysis for paralleled boost converters in DC microgrids," *IEEE Trans. Control Syst. Technol.*, vol. 29, no. 1, pp. 385–394, Jan. 2021, doi: [10.1109/TCST.2019.2951092](https://doi.org/10.1109/TCST.2019.2951092).
- [17] P. Wang, X. Lu, X. Yang, W. Wang, and D. G. Xu, "An improved distributed secondary control method for DC microgrids with enhanced dynamic current sharing performance," *IEEE Trans. Power Electron.*, vol. 31, no. 9, pp. 6658–6673, Sep. 2016, doi: [10.1109/TPEL.2015.2499310](https://doi.org/10.1109/TPEL.2015.2499310).
- [18] L. Zhang, H. Zheng, Q. Hu, B. Su, and L. Lyu, "An adaptive droop control strategy for islanded microgrid based on improved particle swarm optimization," *IEEE Access*, vol. 8, pp. 3579–3593, 2020, doi: [10.1109/ACCESS.2019.2960871](https://doi.org/10.1109/ACCESS.2019.2960871).
- [19] Y. Fu, Z. Zhang, Y. Mi, Z. Li, and F. Li, "Droop control for DC multi-microgrids based on local adaptive fuzzy approach and global power allocation correction," *IEEE Trans. Smart Grid*, vol. 10, no. 5, pp. 5468–5478, Sep. 2019, doi: [10.1109/TSG.2018.2883559](https://doi.org/10.1109/TSG.2018.2883559).
- [20] H. Liu, Y. Wang, M. Wang, Y. Guo, J. Wang, G. Shen, and G. Liao, "Small-signal analysis of DC microgrid and multi-objective optimization segmented droop control suitable for economic dispatch," *J. Mod. Power Syst. Clean Energy*, vol. 8, no. 3, pp. 564–572, 2020, doi: [10.35833/MPCE.2018.000878](https://doi.org/10.35833/MPCE.2018.000878).
- [21] F.-J. Lin, K.-H. Tan, C.-F. Chang, M.-Y. Li, and T.-Y. Tseng, "Development of intelligent controlled microgrid for power sharing and load shedding," *IEEE Trans. Power Electron.*, vol. 37, no. 7, pp. 7928–7940, Jul. 2022, doi: [10.1109/TPEL.2022.3152167](https://doi.org/10.1109/TPEL.2022.3152167).
- [22] S. M. Chowdhury, M. O. Badawy, Y. Sozer, and J. A. D. A. Garcia, "A novel battery management system using the duality of the adaptive droop control theory," *IEEE Trans. Ind. Appl.*, vol. 55, no. 5, pp. 5078–5088, Sep. 2019, doi: [10.1109/TIA.2019.2919497](https://doi.org/10.1109/TIA.2019.2919497).
- [23] C. Guo, J. Liao, and Y. Zhang, "Adaptive droop control of unbalanced voltage in the multi-node bipolar DC microgrid based on fuzzy control," *Int. J. Electr. Power Energy Syst.*, vol. 142, Nov. 2022, Art. no. 108300, doi: [10.1016/j.ijepes.2022.108300](https://doi.org/10.1016/j.ijepes.2022.108300).
- [24] X. Lu, K. Sun, J. M. Guerrero, J. C. Vasquez, and L. Huang, "Double-quadrant state-of-charge-based droop control method for distributed energy storage systems in autonomous DC microgrids," *IEEE Trans. Smart Grid*, vol. 6, no. 1, pp. 147–157, Jan. 2015, doi: [10.1109/TSG.2014.2352342](https://doi.org/10.1109/TSG.2014.2352342).
- [25] T. R. Oliveira, W. W. A. G. Silva, and P. F. Donoso-Garcia, "Distributed secondary level control for energy storage management in DC microgrids," *IEEE Trans. Smart Grid*, vol. 8, no. 6, pp. 2597–2607, Nov. 2017, doi: [10.1109/TSG.2016.2531503](https://doi.org/10.1109/TSG.2016.2531503).
- [26] T. Morstyn, A. V. Savkin, B. Hredzak, and V. G. Agelidis, "Multi-agent sliding mode control for state of charge balancing between battery energy storage systems distributed in a DC microgrid," *IEEE Trans. Smart Grid*, vol. 9, no. 5, pp. 4735–4743, Sep. 2018, doi: [10.1109/TSG.2017.2668767](https://doi.org/10.1109/TSG.2017.2668767).
- [27] M. A. Hannan, Z. A. Ghani, M. M. Hoque, P. J. Ker, A. Hussain, and A. Mohamed, "Fuzzy logic inverter controller in photovoltaic applications: Issues and recommendations," *IEEE Access*, vol. 7, pp. 24934–24955, 2019, doi: [10.1109/ACCESS.2019.2899610](https://doi.org/10.1109/ACCESS.2019.2899610).
- [28] H. Kakigano, Y. Miura, and T. Ise, "Distribution voltage control for DC microgrids using fuzzy control and gain-scheduling technique," *IEEE Trans. Power Electron.*, vol. 28, no. 5, pp. 2246–2258, May 2013, doi: [10.1109/TPEL.2012.2217353](https://doi.org/10.1109/TPEL.2012.2217353).
- [29] N. L. Diaz, T. Dragičević, J. C. Vasquez, and J. M. Guerrero, "Intelligent distributed generation and storage units for DC microgrids—A new concept on cooperative control without communications beyond droop control," *IEEE Trans. Smart Grid*, vol. 5, no. 5, pp. 2476–2485, Sep. 2014, doi: [10.1109/TSG.2014.2341740](https://doi.org/10.1109/TSG.2014.2341740).
- [30] J.-J. Yan, G.-H. Yang, and X.-J. Li, "Adaptive fault-tolerant compensation control for T-S fuzzy systems with mismatched parameter uncertainties," *IEEE Trans. Syst., Man, Cybern., Syst.*, vol. 50, no. 9, pp. 3412–3423, Sep. 2020, doi: [10.1109/TSMC.2018.2854630](https://doi.org/10.1109/TSMC.2018.2854630).
- [31] X. Sun and Q. Zhang, "Observer-based adaptive sliding mode control for T-S fuzzy singular systems," *IEEE Trans. Syst., Man, Cybern., Syst.*, vol. 50, no. 11, pp. 4438–4446, Nov. 2020, doi: [10.1109/TSMC.2018.2852957](https://doi.org/10.1109/TSMC.2018.2852957).
- [32] H. Ying, "Constructing nonlinear variable gain controllers via the Takagi–Sugeno fuzzy control," *IEEE Trans. Fuzzy Syst.*, vol. 6, no. 2, pp. 226–234, May 1998, doi: [10.1109/91.669021](https://doi.org/10.1109/91.669021).



**MAO JINGFENG** received the B.Eng. degree in industrial automation from the School of Automation, Wuhan University of Technology, Wuhan, China, in 1998, and the M.Sc. and Ph.D. degrees in electrical engineering from the School of Electrical and Information Engineering, Jiangsu University, Zhenjiang, China, in 2004 and 2008, respectively.

Since 1998, he has been with Nantong University, Nantong, China, where he is currently a Professor with the School of Electrical Engineering. His current research interests include electrical machines and drives, renewable energy generations and applications, and control and design of microgrids.



**ZHANG XIAOTONG** received the B.Eng. degree in electrical engineering and automation from the School of Electrical Engineering, Nantong University, Nantong, China, in 2020, where she is currently pursuing the M.Sc. degree. Her current research interest includes DC microgrid operation and control.

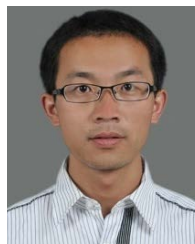


**YIN CHUNYUN** received the B.Eng. degree in electrical engineering and intelligent control from the School of Electrical Engineering, Nantong University, Nantong, China, in 2020, where he is currently pursuing the M.Sc. degree. His current research interest includes DC microgrid control.



**WU AIHUA** received the B.Eng. degree in industrial automation from the School of Electrical Engineering, Nantong University, Nantong, China, in 2000, the M.Sc. degree in electrical engineering from the School of Automation, Nanjing University of Aeronautics and Astronautics, Nanjing, China, in 2006, and the Ph.D. degree in electrical engineering from the School of Electrical and Information Engineering, Jiangsu University, Zhenjiang, China, in 2019.

Since 2000, she has been with Nantong University, where she is currently an Associate Professor with the School of Mechanical Engineering. Her current research interests include electrical machines and drives and renewable energy generations and applications.



**ZHANG XUDONG** received the B.Eng. degree in electrical engineering and automation and the M.Sc. degree in control theory and control engineering from the School of Electrical Engineering, Nantong University, Nantong, China, in 2007 and 2010, respectively.

Since 2010, he has been with Nantong University, where he is currently a Lecturer with the School of Electrical Engineering. His current research interest includes renewable energy generations and applications.

• • •